Manifestation of the statistical nature of a medium in multiple small-angle scattering

2001 J. Phys.: Condens. Matter 13 5089

(http://iopscience.iop.org/0953-8984/13/22/306)

INSTITUTE OF PHYSICS PUBLISHING JOURNAL OF PHYSICS: CONDENSED MATTER

J. Phys.: Condens. Matter **13** (2001) 5089–5102 www.iop.org/Journals/cm PII: S0953-8984(01)18796-5

Manifestation of the statistical nature of a medium in multiple small-angle scattering

S Mazumder[1], D Sen[1], S K Roy[2], M Hainbuchner[3], M Baron[3,4] and H Rauch[3]

[1] Solid State Physics Division, Bhabha Atomic Research Centre, Mumbai 400 085, India
[2] Materials Science Division, Bhabha Atomic Research Centre, Mumbai 400 085, India
[3] Atominstitut der Osterreichischen Universitaten, A-1020 Wien, Austria
[4] Institut Laue–Langevin, Grenoble, France

E-mail: smau@apsara.barc.ernet.in (S Mazumder)

Received 7 November 2000, in final form 2 March 2001

Abstract

It has been emphasized in the recent past that the beam-broadening feature of multiple scattering can be used to investigate large inhomogeneities which are otherwise inaccessible by means of small-angle scattering due to the inherent resolution constraint. However, the treatment of data on multiple small-angle scattering from a polydisperse sample needs more critical evaluation. As multiple small-angle scattering deals with large inhomogeneities, the scattering mean free path L may not be appreciably large in comparison to the linear dimension R of the inhomogeneities for many systems. When $L \gg R$, the scattering medium can be treated in a mean-field way and such a medium has been termed an 'effective medium'. But when the condition $L \gg R$ does not hold, the statistical nature of the medium is manifested. The manifestation is a modulation of the multiple-scattering profile compared with that from an effective medium. In the present paper, we report for the first time an experimental demonstration of the manifestation of the statistical nature of the medium in an experiment based on multiple small-angle neutron scattering on sintered alumina with varying sample thickness. The effect of the statistical nature of the medium has been observed for $L/R > 1000$.

1. Introduction

In traditional small-angle scattering (SAS) experiments using 'thin samples', scattering data are interpretable in terms of laws based on single-scattering approximation. In such cases the functionality or shape of the scattering profile is invariant with respect to sample thickness or wavelength of the probing radiation. In other words, the scattering profiles recorded with variation of sample thickness or wavelength are different as regards a scale factor only. They become indistinguishable from each other after suitable normalization and also when the absolute intensities are used to represent the scattering profiles.

0953-8984/01/225089+14$30.00

SAS data from porous systems are often affected by multiple scattering. The influence of multiple scattering in SAS data arises due to one or more of these factors: strong contrast, long wavelength, large inhomogeneities and significant thickness of the sample. Very often factors like strong contrast, long wavelength and large inhomogeneities reduce the scattering mean free path (SMFP) L to such an extent that there is gross violation of the single-scattering approximation which demands that thickness should be infinitesimally small in comparison to the SMFP. But often samples supposed to replicate the bulk matrix in essential properties are too thick for the single-scattering approximation to be valid. The choice of long wavelength in scattering experiments is due to two factors, namely, the possibility of carrying out measurements at smaller wave-vector transfer and its elimination effect on components such as double Bragg reflections in the signal.

The signature of multiple scattering is the functional dependence of measured profiles on the sample thickness or the wavelength of the probing radiation. A primary feature of multiple scattering is the broadening of the scattering profile. Some of the recent literature [1–5] emphasizes that the beam-broadening feature of multiple scattering can be exploited in SAS experiments to probe large inhomogeneities which are otherwise inaccessible to SAS study due to its inherent resolution constraint. As a result of the relatively large thickness of the sample in a multiple-scattering experiment, the incident beam will be scattered almost completely, yielding much improved signal-to-noise ratio up to very high wave-vector transfers. Such exploitation of multiple scattering is only possible when the full implications of the size R of the inhomogeneities in relation to the scattering mean free path L for the multiple-scattering profile are appreciated.

Many of the scattering systems pertinent to materials science are polydisperse in nature. As multiple small-angle scattering (MSAS) deals with large inhomogeneities, the scattering mean free path L may not be appreciably large in comparison to the linear dimension R of the inhomogeneities for many systems. It is important to note that the number density of the inhomogeneities and all other parameters like wavelength λ and scattering length density difference D remain unchanged; $L \sim R^{-4}$. When $L \gg R$, the scattering medium can be treated in a mean-field way and such a medium has been termed an 'effective medium' (see figure 1). But when the condition $L \gg R$ does not hold, the statistical nature of the medium is manifested and such a medium is termed a 'statistical medium' [6, 7]. Although ascertaining a numerical value of L/R for which the effective-medium approximation holds good is beyond the scope of the theory, computations of scattering profiles with and without the effective-medium approximation for different model systems are helpful for getting a quantitative estimate of the modulation effect of the statistical nature of the medium.

The computations of profiles of scattering from polydisperse media can be carried out under different approximation schemes like the effective-medium approximation and the small-noise approximation [8]. It is also possible to extract some information about the inhomogeneities from experimental data under the aforementioned approximations. The computation of the profile of scattering from a model bidisperse statistical medium has already been dealt with [7, 9, 10]. It has been shown that the effect of the statistical nature of the medium is to modulate the scattering profile in comparison to that for an effective medium. The nature of the modulation could be either broadening or narrowing of the profile depending upon the characteristics of the statistical medium. But the computation of profiles for polydisperse statistical media has not been performed so far, due to the cumbersome algebra. An algorithm for analysing multiple-SAS data from a statistical medium is yet to be developed and such an algorithm will extend the usefulness of the SAS technique to a large extent, with new applications in materials research.

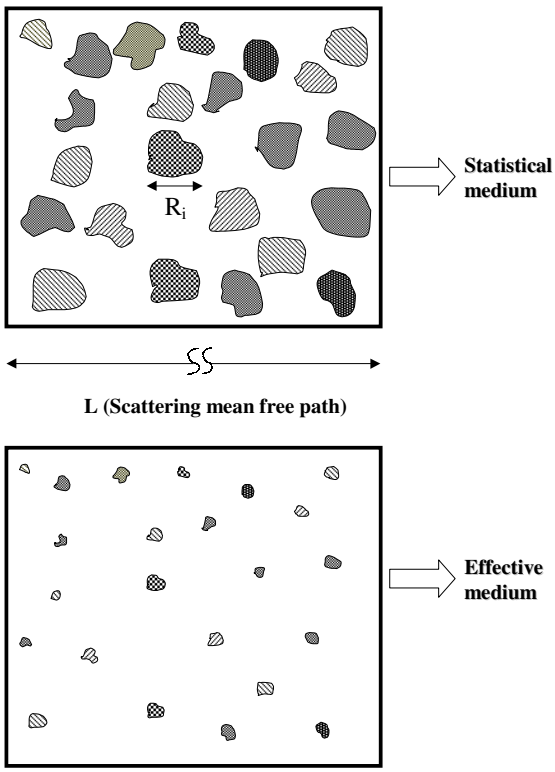

Figure 1. A schematic representation of the statistical and effective scattering media. In an effective medium, the linear dimensions of the inhomogeneities are negligibly small in comparison to the scattering mean free path. But this is not so for the case of a statistical medium.

Experimental work demonstrating the effect of the statistical nature of a medium is yet to be reported and this work can be seen as a step in that direction.

In the present work, we have carried out high-resolution small-angle neutron scattering (SANS) experiments on three specimens of sintered alumina of varying thickness. The aim is to find out to what extent the description of multiple small-angle scattering under the effective-medium approximation (EMA) is consistent with the recorded scattering profiles of these specimens. Under conditions where the EMA is applicable, it is possible [11, 12] to predict the scattering profile of a specimen of defined thickness from two profiles recorded with two different thicknesses of the same specimen, by first estimating the scattering mean free path and then estimating of true single-scattering profile of the specimen.

2. Experiment

2.1. Samples

Specimens of right cylinder geometry of nearly 1.44 cm diameter and different thicknesses were prepared by cutting a sintered billet with a diamond saw. The various steps in the preparation of specimens are as follows:

- α-Al_2O_3 powder having the median diameter (D_{50}) of 0.61 μm and specific surface area of 118 864 cm^2 cm^{-3} was used in this study. An amount of aqueous $Mg(NO_3)_2{\cdot}H_2O$

equivalent to 0.2% by weight of MgO was homogeneously mixed with this powder to act as a grain growth inhibitor.

- The powder was wet ground in kerosine for 24 hours in a polyethylene jar mill with zirconia milling media to disperse the particles completely. Oleic acid was used as the grinding aid (1% by weight). The binder phase consisting of paraffin wax (major binder), beeswax (minor binder) and stearic acid (plasticizer) was hot mixed with the above at 60 °C. Mixing of the binder phase and the dispersed powder was carried out in a planetary mixer. Liquid medium was removed by vacuum evaporation at 60 °C while agitating continuously inside the mixer. The material was subsequently granulated by forcing the mass through a sieve of BS-100 mesh.
- The granules were filled into a die and compacted uniaxially under a pressure of 140 MPa in a laboratory hydraulic press to form right circular cylindrical billets. Compacted billets were put into a programmable furnace with $MoSi_2$ heating elements and heated in air at the rate of 100 °C h^{-1} to 650 °C with a two-hour soaking period. Sintering was carried out at 1600 °C in air for two hours.
- Bulk densities of the sintered specimens were determined by the liquid displacement method using xylene as the suspending liquid. The sintered density of these specimens was found to be 3.63 g cm^{-3} (91% of the theoretical density). Three specimens of circular cross section and thicknesses of 0.650, 0.306 and 0.272 cm respectively were cut from a sintered billet with a diamond circular saw. The bulk densities of these individual specimens were found to be nearly equal to that of the billet, i.e., 91% of theoretical density.

2.2. SANS experiments

The SANS experiments were carried out at the ultrasmall-angle neutron scattering instrument [13] S18 at the 58 MW high-flux reactor at the Institute Laue–Langevin in Grenoble, France. The neutron flux density measured at the sample position with this Bonse–Hart-type [14] camera is about 10 000 neutrons cm^{-2} and the signal-to-noise ratio is better than 10^5. The wavelength λ used is 1.87 Å. The scattered intensities were recorded as a function of q ($=4\pi(\sin\theta)/\lambda$, 2θ being the scattering angle). At zero angle, the Bonse–Hart analyser passes the full intensity of the straight-through beam; hence the measured transmission T is the ratio of the intensities at zero angle with and without the sample. For a Bonse–Hart camera, the transmission T is a measure of the total linear removal cross section Σ_{tot} of the sample. It is given by the following relation:

$$T = \exp(-t\,\Sigma_{tot}) \tag{1}$$

where t is the specimen thickness and Σ_{tot} is the total linear removal cross section of the sample. For a sample undergoing only small-angle scattering and absorption, Σ_{tot} is given by

$$\Sigma_{tot} = L^{-1} + \mu \tag{2}$$

where L is the scattering mean free path and μ is the linear absorption cross section of the sample.

The measured scattering profile $I_M(q)$ of a specimen is given by the following relation:

$$I_M(q) = T\left\{I_0(q) + C\int \mathrm{d}q_v\; W_V(q_v)t\frac{\mathrm{d}\Sigma}{\mathrm{d}\Omega}(\sqrt{q^2+q_v^2})\right\} + B \tag{3}$$

where $I_0(q)$ is the measured scattering profile for the direct beam; q_v is the component of q in the vertical direction; $\mathrm{d}\Sigma(q)/\mathrm{d}\Omega$ is the desmeared differential scattering cross section of the specimen per unit volume per unit solid angle; $W_V(q)$ is the normalized resolution function of

the instrument along the vertical direction in q-space; t is the specimen thickness; C is a scale factor independent of q; and B is the background arising due to scattering from air, slits and other possible sources including incoherent scattering from the crystals.

So the transmission-corrected and background-corrected recorded scattering profile $I(q)$ of the specimen is given by

$$I(q) = \int \mathrm{d}q_v \; W_V(q_v) S\left(\sqrt{q^2 + q_v^2}\right) \tag{4}$$

where $S(q)$ is the desmeared scattering profile of the specimen on an arbitrary scale.

In the present work, the intensities were corrected for sample absorption and smearing effects [15] to get an estimate of $S(q)$. For the present discussions, the scattering profiles of the specimens on an absolute scale are not required. The scattering data have been normalized to the same intensity at the lowest attainable q-value and calculations have been carried out with the normalized intensities.

3. Data interpretation and discussion

Figure 2 shows scattering profiles of the three specimens. A normalized scale of intensities has been used to depict the thickness dependence of the functionalities of the profiles. The intensities of the individual scattering profiles are fixed at 1.0 at the lowest q-value

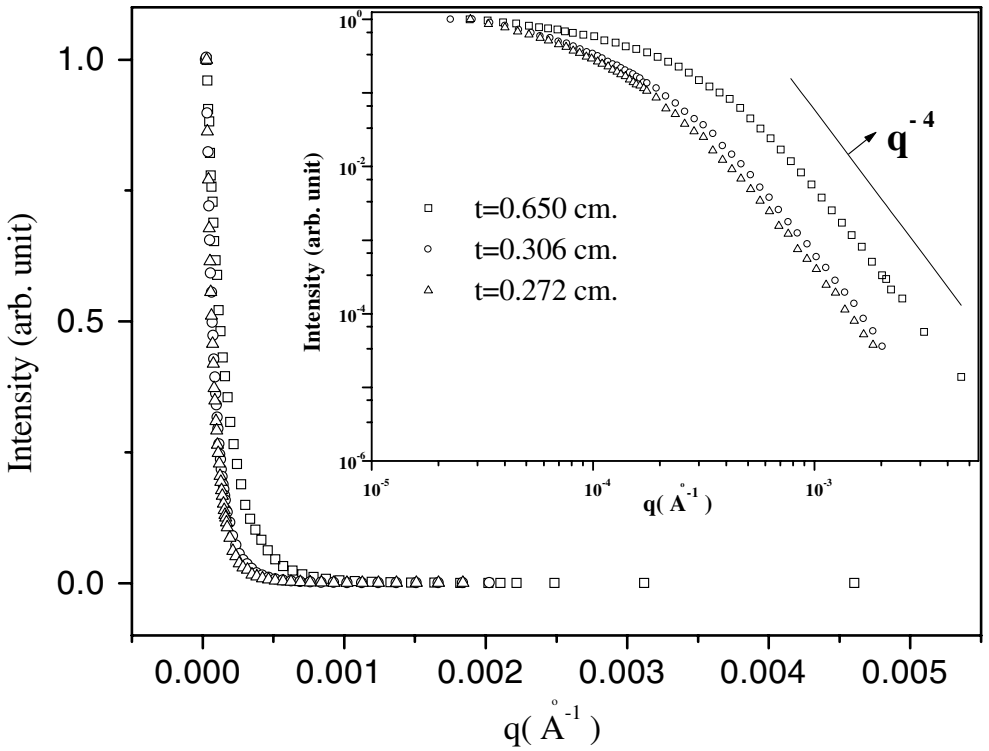

Figure 2. Recorded scattering profiles of the three specimens varying in thickness. To show the distinctiveness of the profiles, a normalized scale has been used. The error bars are smaller than the size of the symbols. At large q, the profiles follow a power law $\sim q^{-4}$. The solid line is only a guide to the eye.

($\sim 3.345 \times 10^{-5}$ Å^{-1}) accessed in these measurements. It is important to note that in conventional small-angle scattering, where the single-scattering approximation holds, variation of the sample thickness or wavelength does not change the profile; i.e., the profiles are different as regards a scaling factor only.

It is evident from figure 2 that with increasing thickness the curvature of the scattering profiles in the vicinity of $q \to 0$ decreases. The curvature κ of the scattering profile $I(q)$ at q is given by

$$\kappa = \frac{|\mathrm{d}^2 I(q)/\mathrm{d}q^2|}{[1 + (\mathrm{d}I(q)/\mathrm{d}q)^2]^{3/2}}. \tag{5}$$

κ is a measure of the negative gradient of the Guinier plot of the scattering profile. For a single-scattering profile for scattering from a monodisperse population of spheres of radius R, $\kappa = 2R^2/5$. For dominant [9] multiple scattering from a monodisperse population of spheres, $\kappa = 2R^2/(5N)$ where N ($=t/L$, the ratio of sample thickness t to the scattering mean free path L) is a statistical number signifying the average number of scattering interactions that radiation has undergone while passing through the sample. It is related to the absolute scattering cross section $\mathrm{d}\Sigma(q)/\mathrm{d}\Omega$ by the following relation:

$$\int \mathrm{d}\Omega \, \frac{\mathrm{d}\Sigma}{\mathrm{d}\Omega}(q) = \frac{1 - \exp(-N)}{t}. \tag{6}$$

For very thin samples,

$$\int \mathrm{d}\Omega \, \frac{\mathrm{d}\Sigma}{\mathrm{d}\Omega}(q) \approx L^{-1} \tag{7}$$

and under the small-angle approximation,

$$\int \mathrm{d}q \, q \frac{\mathrm{d}\Sigma}{\mathrm{d}\Omega}(q) \sim L^{-1}\lambda^{-2}. \tag{8}$$

In the diffraction limit [15], $L \sim \lambda^{-2}$ and hence, for very thin samples, $\mathrm{d}\Sigma(q)/\mathrm{d}\Omega$ is independent of t and λ.

The fraction $\zeta(n, N)$ of incident radiation undergoing n scattering events while passing through the sample of thickness t is given by $\zeta(n, N) = \exp(-N)N^n/n!$.

The scattering mean free path L can be estimated for a few model systems. For a polydisperse population of spherical scatters, with number density $\rho(R)$ for scatterers of radius R, having the same scattering length density difference D, L is given [16] by

$$L = \left\{ 2\pi \left[\int_0^\infty \rho(R) R^2 f(\gamma) \, \mathrm{d}R \right] \right\}^{-1} \tag{9}$$

where

$$f(\gamma) = 1 - (2/\gamma^2)[\gamma \sin(\gamma) + \cos(\gamma) - 1]$$
$$\gamma = 2\lambda D R$$

and λ is the wavelength of the probing radiation.

When $\gamma \ll 1$ (the diffraction limit [15]), the above expressions for $f(\gamma)$ and L reduce to

$$f(\gamma) \approx (\gamma/2)^2$$

and

$$L = \frac{2\langle R^3 \rangle}{3D^2\lambda^2\phi\langle R^4 \rangle} \tag{10}$$

where ϕ is the packing fraction of the scatterer in the specimen and $\langle R^n \rangle$ is the nth moment of the distribution $\rho(R)$.

The effect of multiple scattering and the data analysis procedure depends upon the degree of multiple scattering which is conveniently measured by N. For a sample undergoing only small-angle scattering and absorption, with linear absorption coefficient μ, N is related to the true transmission T of the sample by the relation

$$T = \exp(-N - \mu t). \tag{11}$$

Transmission as measured in the experiment is somewhat overestimated because of the contamination of the scattering signal with the true transmitted component of the radiation passing through the sample. The overestimation of transmission from measurement becomes quite appreciable for measurements significantly affected by multiple scattering. Thus only N-values estimated from transmission measurements will be underestimated. The underestimation will be more for measurements significantly affected by multiple scattering.

The estimated values of $\kappa/2$ and N (based on transmission measurements only) for the three scattering profiles along with the measured transmission of the specimens are listed in table 1. It is pertinent to note that $\mu \approx 0.01$ cm^{-1} for alumina samples with 91% theoretical density for neutrons with $\lambda = 1.87$ Å.

Table 1. The estimated $\kappa/2$ values, the Porod exponents, the measured transmission T and the N-values estimated from transmission measurements for the three specimens. The numbers in parentheses denote the estimated standard deviation values of the relevant quantities.

Sample thickness (cm)	$\kappa/2$ (10^8 Å^2)	Porod exponent	T (%)	N (estimated from T only)	N (estimated with the assumption that $L = 0.064$ (0.007) cm)
0.272 (0.001)	2.912 (0.175)	3.99 (0.28)	94.98 (0.19)	0.049 (0.003)	4.25 (0.109)
0.306 (0.001)	1.997 (0.129)	4.01 (0.28)	92.89 (0.19)	0.071 (0.002)	4.781 (0.109)
0.650 (0.001)	1.002 (0.070)	3.98 (0.32)	78.99 (0.16)	0.229 (0.002)	10.156 (0.109)

Porod exponents, as estimated from ln(intensity) versus ln(q), in the q-range beyond $q = 0.001$ Å^{-1} for various specimens are also listed in table 1. The scattering profiles follow a power law, $\sim q^{-4}$. It is noteworthy that the functional dependence of the scattered intensity in the Porod region of the momentum-transfer vector remains invariant [7, 9, 10] under multiple scattering irrespective of the nature of the scattering medium.

Now, at the outset let us examine to what extent the recorded scattering profiles of the specimens can be interpreted in terms of polydisperse spherical pores without accounting for the multiple-scattering effects. The recorded profiles are best interpreted in terms of radius dispersion $\rho(R)$ of the pores in the form of a log-normal distribution:

$$\rho(R) = \frac{1}{\sqrt{2\pi\sigma^2 R^2}} \exp\left[\frac{-[\ln(R/R_0)]^2}{2\sigma^2}\right]$$

where R_0 and σ are adjustable parameters. The results of the fit as well as the mean free path of neutrons with $\lambda = 1.87$ Å, both under the diffraction limit and otherwise, estimated from the distributions obtained are given in table 2. For estimation of L, the packing fraction ϕ and scattering length density difference D of the pores in the specimens have been considered to be respectively $9 \pm 0.06\%$ and 5.726×10^{-6} Å^{-2}. The choice of $9 \pm 0.06\%$ pore volume fraction is based on bulk density measurement. Figure 3 shows the comparison between the recorded profiles and the theoretical profiles calculated back from the estimated R_0 and σ of the log-normal distribution of the pores.

The present method of estimation [11, 12] of the scattering mean free path L is based on the principle that although different multiple-scattering profiles for different specimen

Table 2. The results from the fit of the polydisperse spherical pores following log-normal distribution and the estimated mean free path L under the diffraction limit and otherwise from the recorded profiles of three specimens before accounting for multiple-scattering effects. The parameters are defined in the text. The numbers in parentheses denote the estimated standard deviation values of the relevant quantities.

Profile specification (thickness (cm))	R_0 (Å)	σ	$\langle R \rangle$ (Å)	$\langle R^2 \rangle$ (10^6 Å^2)	L (equation (9)) (cm)	L (diffraction limit, equation (10)) (cm)
0.272 (0.001)	858 (25)	0.794 (0.027)	1176 (55)	2.60 (0.14)	0.084 (0.005)	0.083 (0.005)
0.306 (0.001)	835 (25)	0.775 (0.023)	1129 (52)	2.32 (0.13)	0.095 (0.006)	0.095 (0.006)
0.650 (0.001)	544 (17)	0.742 (0.022)	717 (33)	0.89 (0.05)	0.174 (0.009)	0.173 (0.009)

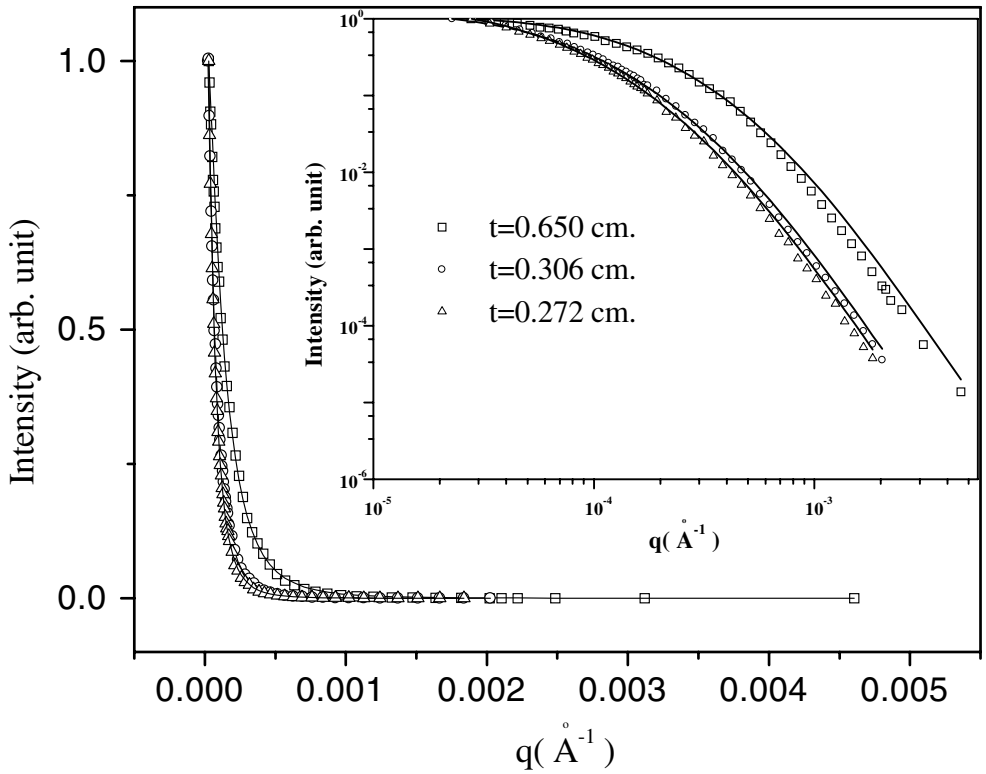

Figure 3. The comparison between the recorded profiles and the theoretical profiles calculated from the estimated R_0 and σ, as shown in table 2, of the log-normal distribution of the pores.

thicknesses are functionally distinct, the computed single-scattering profiles for each of them are functionally the same or least deviated provided that the correct L-value is used for the inversion. The method is not model specific as regards the scattering medium other than the fact that it works successfully only for an effective medium. It has been demonstrated [12] that it works also when there is a strong spatial correlation among the inhomogeneities. The method involves Hankel transformation of recorded profiles. It uses interpolations of data points and extrapolations of the profiles in the extremum domains of q. For successful numerical integrations, it is important that the recorded data points are sufficiently close for

achieving faithful interpolations and the recorded data sets are complete to enable realistic extrapolations. Factors like improper extrapolations of the recorded profiles, improper choice of the integration limits or the sample not satisfying the effective-medium approximation can give rise to some inadequacies. The violation of the effective-medium approximation becomes more serious with increase of the wavelength, as the scattering mean free path L ($\sim\lambda^2$) decreases exponentially.

To begin the treatment of the scattering data affected by multiple scattering, we assume the scattering medium to be an effective medium. This will also highlight the inconsistencies brought about by the assumption. Since profiles for the thinner samples are less affected by multiple scattering, two profiles for specimens of thickness 0.272 and 0.306 cm are chosen for the estimation of the scattering mean free path L. The mean free path L has been estimated to be 0.064 ± 0.007 cm. Subsequently, it will be considered that the actual value of the mean free path could be somewhat more. Further, the estimated L-values are less than the tabulated L-values, as shown in table 2, from the recorded profiles of specimens. The latter observation is expected, as the recorded profiles are affected by multiple scattering, whose essential effect in the present experiment is to broaden the scattering profile. Hence, it is only to be expected that if multiple-scattering effects are not accounted for, the conventional data analysis will lead to an underestimation of the linear dimension of the particles. Underestimation of the linear dimension leads to overestimation of the L-value.

With $L = 0.064 \pm 0.007$ cm, the single-scattering profile estimated from the profile of the 0.272 cm thick specimen under the effective-medium approximation is shown in figure 4.

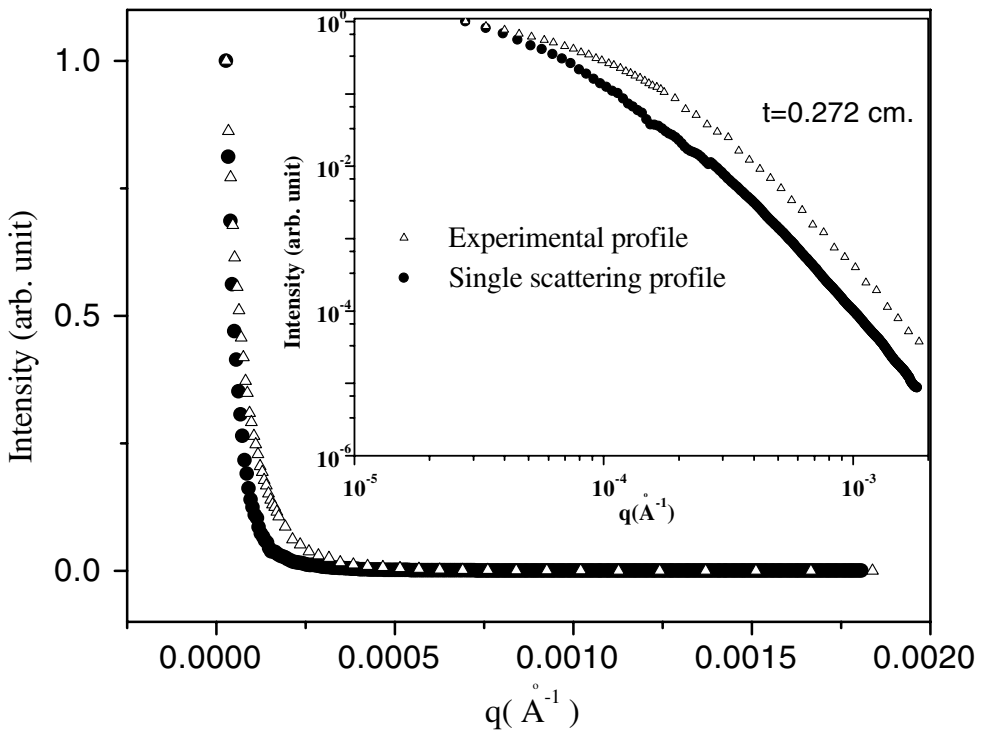

Figure 4. A comparison of profiles—namely, the estimated single-scattering profile and the recorded profile for a specimen of thickness 0.272 cm. The error bars are smaller than the size of the symbols.

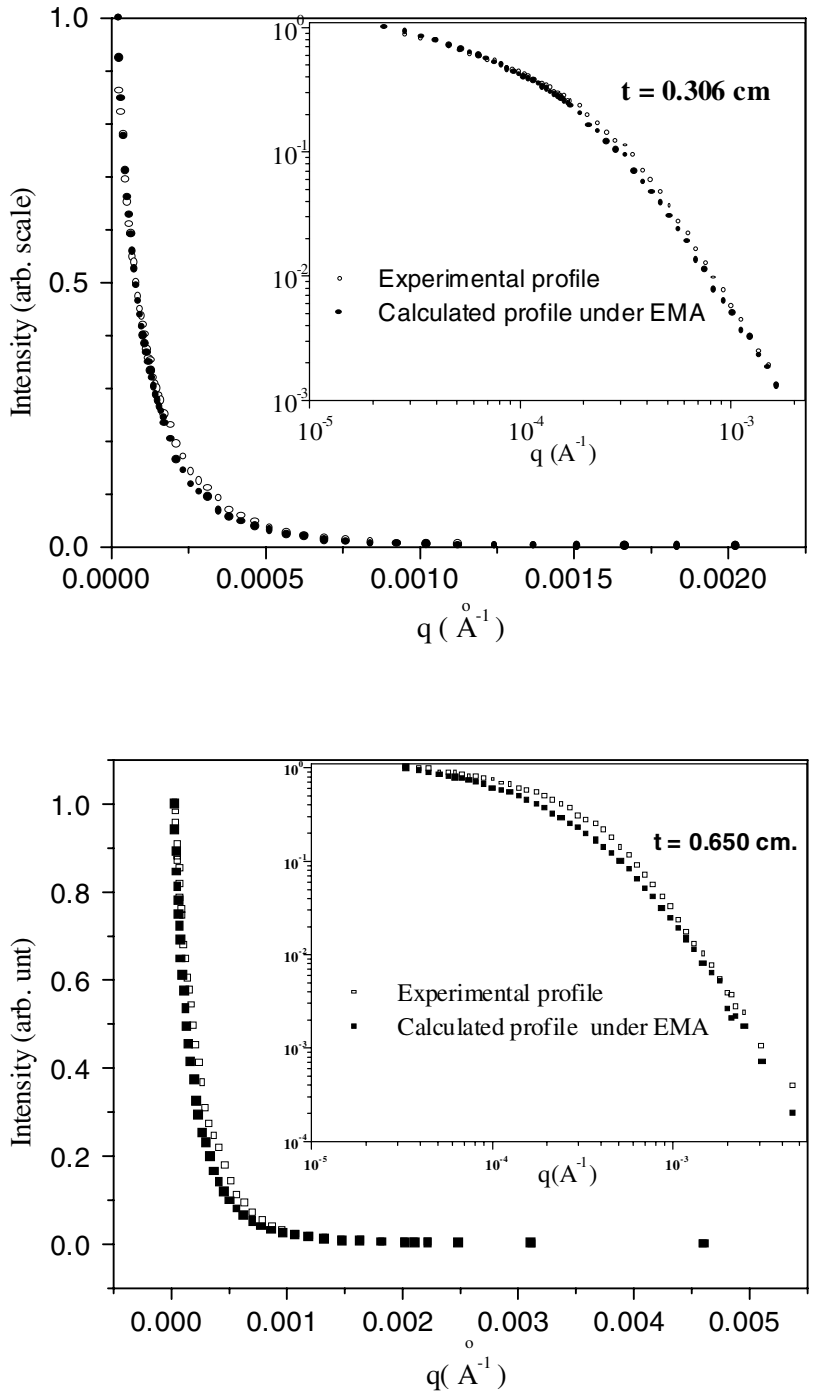

Figure 5. A comparison of the recorded profiles for specimens of thicknesses 0.306 and 0.650 cm and the profile calculated for the same specimen, under the effective-medium approximation, using the estimated single-scattering profile, scattering mean free path and sample thickness. The error bars are smaller than the size of the symbols.

It is expected that the estimated single-scattering profile will be sharper compared with the recorded profiles affected by multiple scattering.

To check the validity of the effective-medium approximation (EMA) in the present case, we have calculated, with this L, the expected multiple-scattering profiles for specimens of thicknesses 0.306 and 0.650 cm, under the EMA, from the estimated single-scattering profile. The calculated profiles compared with the experimentally recorded profiles are shown in figure 5. It is evident from these figures that the experimental profiles are broader than the calculated profiles. The thicker the specimen, the greater the difference between the experimental and calculated profiles. It is also evident that in the present specimens, the effect of the statistical nature of the medium is to broaden the scattering profile compared with the one expected under the EMA.

Figure 6 depicts the variation of $\sqrt{(\kappa/2)}$ versus $\log(N)$ for measured profiles as well as for the profiles calculated under the EMA. The values of $\kappa/2$ have been normalized at $N = 4.25$. This further validates the point that the present specimens do not conform with the EMA.

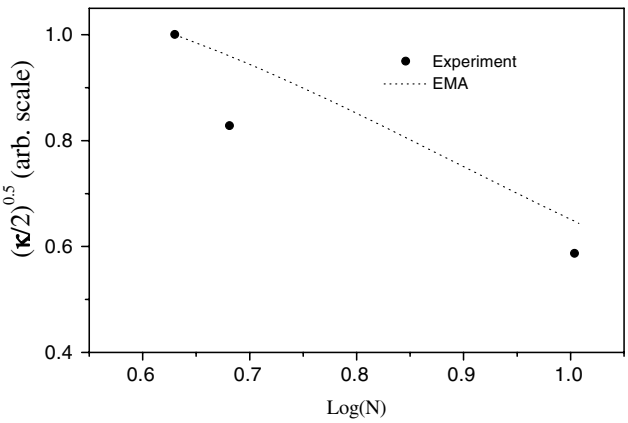

Figure 6. Variation of the estimated curvature of the scattering profiles with N. Filled circles show the variation for the recorded profiles while the dotted curve shows the variation for the profiles calculated, under the effective-medium approximation, using the estimated single-scattering profile and assumed N-values.

To illustrate the effects of the statistical nature of the medium on scattering profiles affected by multiple scattering and also to explain the qualitative features of the present experimental investigation, the results of some model calculations are presented below.

For model calculations, we have assumed porous alumina samples with 10% porosity containing two sizes of pore with radii of 1000 and 3000 Å. The volume fractions of the pores with radii of 1000 and 3000 Å have been assumed to be 1 and 9%, respectively. To amplify the effect of the statistical nature of the medium, we have assumed $\lambda = 10.0$ Å. In the present model calculations, we have assumed the diffraction limit of scattering throughout for convenience of computation. The qualitative features discussed in the following will not be affected by this assumption.

Under the diffraction limit, the scattering mean free path of such a medium has been estimated to be 0.007 26 cm. Figure 7 depicts the scattering profiles, under the effective-medium approximation and otherwise, for such a medium with thickness 0.306 cm. It is evident that the effect of the statistical nature of the medium is the broadening of the profile compared with that for an effective medium. From the present and previous [7, 9] model calculations, it is evident that the statistical nature of the medium is manifest even for $L > 100R$. The theory

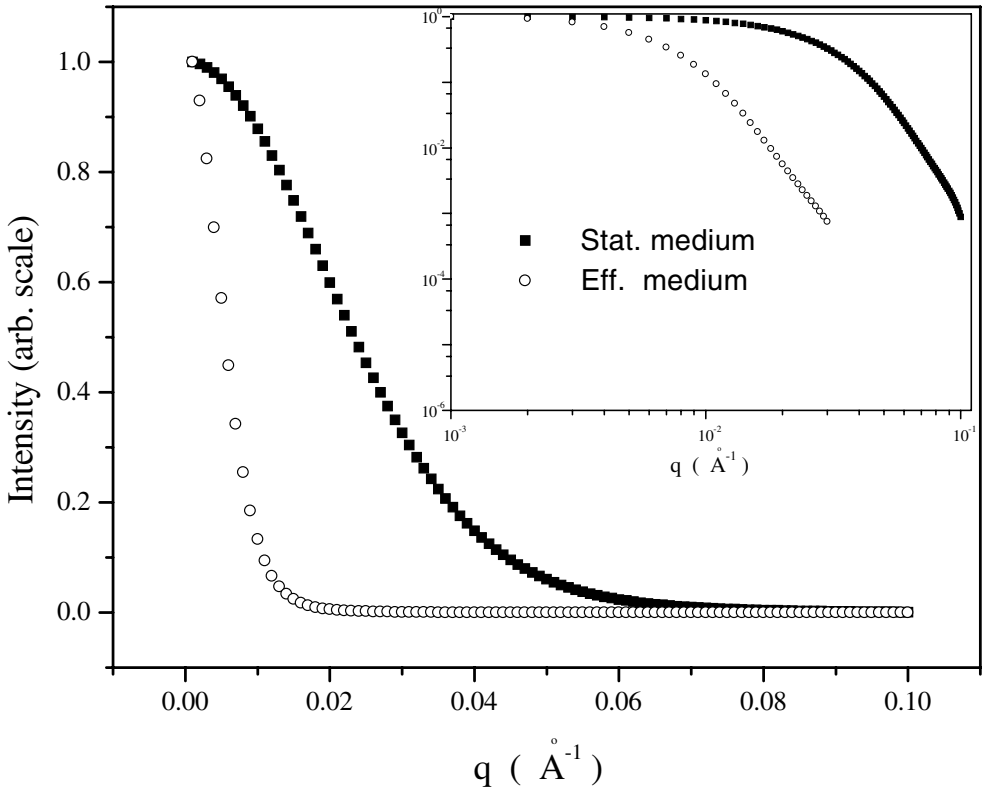

Figure 7. Scattering profiles computed, with and without the effective-medium approximation, for a model system as described in the text. The inset shows the calculated profiles on a log–log scale.

[6–10] of multiple small-angle scattering from a statistical medium indicated that when the linear dimensions of the inhomogeneities are negligibly small in comparison to the scattering mean free path, the effect of the statistical nature of the medium can be ignored. Although ascertaining a numerical value of L/R for which the effective-medium approximation holds good is beyond the scope of the theory directly, it is well within the scope of model calculations and experimental investigations to estimate the modulation effect of the statistical medium, compared with the effective medium, on multiple-scattering profiles.

Figure 8 shows the results of model calculations, with and without effective-medium approximation, on the variation of the measure $\sqrt{(\kappa/2)}$ of curvature of the scattering profiles with thickness of the specimens. These two results indicate the same qualitative trend—namely, the beam-broadening effect of the statistical nature of the medium and the relatively sharper decline of the estimated radius of curvature of the scattering profiles with varying sample thickness, in the present experimental investigation.

To explain why the true L-value for our experimental system could be greater than the estimated value 0.064 ± 0.016 cm, the results of some model calculations are presented below. We have considered the same model scattering system as described above and calculated the scattering profiles for two specimens of thicknesses 0.272 and 0.306 cm. In the present set of calculations, $\lambda = 1.87$ Å has been assumed. Under the diffraction limit, the scattering mean free path has been estimated to be 0.2076 cm. Figure 9 depicts the calculated scattering profiles. Under the effective-medium approximation, the mean free path estimated from the

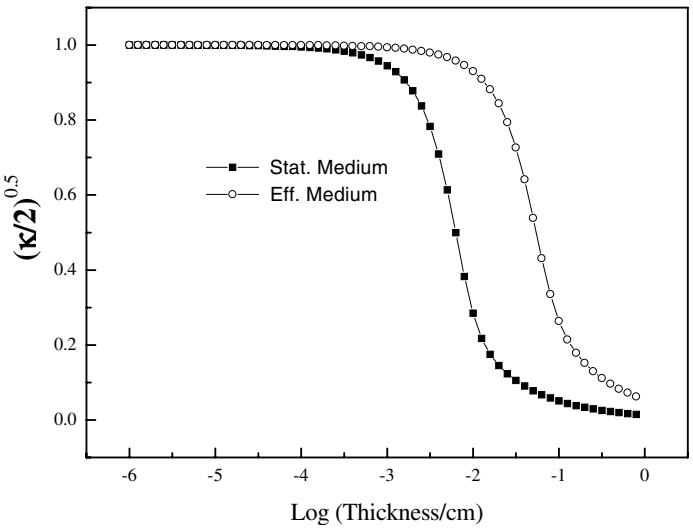

Figure 8. The variation with N of the estimated radius of curvature of the scattering profiles, with and without the effective-medium approximation, for a model system as described in the text.

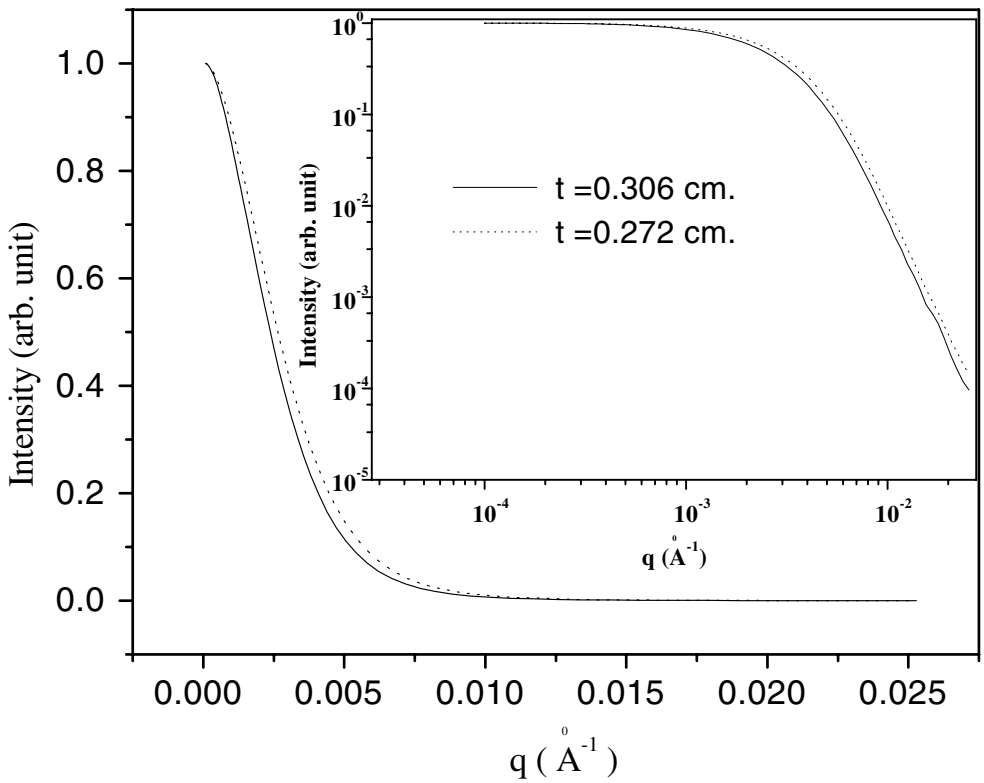

Figure 9. Scattering profiles of a model system, as described in the text, for specimen thicknesses of 0.272 and 0.306 cm.

two theoretical profiles has been found to be 0.168 31 cm, a value somewhat lower than the actual one. Model calculations on estimation of the scattering mean free path from the effective medium, even after imposing random statistical error on the calculated intensities, showed [12] much less deviation of the estimated value from its implicit value.

4. Conclusions

In the present work, it has been demonstrated that there are specimens which are beyond the description of the effective-medium approximation even when the scattering mean free path is larger than the linear dimensions of the inhomogeneities by at least three orders of magnitude. So far these effects have been discussed from the theoretical point of view only and an experimental demonstration was needed. The present experiment serves that purpose. The effect of the statistical nature of the scattering medium becomes more serious for thicker specimens and particularly for measurements employing a larger wavelength of the probing radiation. Recently, the exploitation of some aspects of multiple small-angle scattering has been emphasized both theoretically and experimentally as more high-resolution small-angle neutron scattering facilities are available now for investigating some specimens, like ceramics and cements, of technological relevance. But the manifestation of the statistical nature of the medium must be considered in such exploitation.

Acknowledgments

We gratefully acknowledge Dr S K Sikka for kind support of and keen interest in this work. Financial support towards building the instrument by the EURATOM project ADV1.1.1 is acknowledged as well. We are grateful to the referees for many useful suggestions.

References

[1] Sabine T M and Bertram W K 1999 *Acta Crystallogr.* A **55** 500
[2] Mazumder S and Sequeira A 1999 *Neutron News* **10** (1) 24
[3] Allen A J and Berk N F 1998 *Neutron News* **9** (2) 13
[4] Mazumder S, Sen D, Sastry P U M, Chitra R, Sequeira A and Chandrasekaran K S 1998 *J. Phys.: Condens. Matter* **10** 9969
[5] Mazumder S, Sequeira A, Roy S K and Biswas A R 1993 *J. Appl. Crystallogr.* **26** 357
[6] Mazumder S and Sequeira A 1989 *Phys. Rev.* B **39** 6370
[7] Mazumder S and Sequeira A 1990 *Phys. Rev.* B **41** 6272
[8] Mazumder S and Sequeira A 1991 *Physica* B **174** 200
[9] Mazumder S and Sequeira A 1992 *Pramana* **38** 95
[10] Mazumder S and Sequeira A 1992 *J. Appl. Crystallogr.* **25** 221
[11] Mazumder S, Jayaswal B and Sequeira A 1998 *Physica* B **241–243** 1222
[12] Jayaswal B and Mazumder S *BARC Report* BARC/1998/E/024
[13] Hainbuchner M, Villa M, Kroupa G, Bruckner G, Baron M, Amenitsch H, Seidl E and Rauch H 2000 *J. Appl. Crystallogr.* **33** 851
[14] Bonse U and Hart M 1965 *Appl. Phys. Lett.* **7** 238
[15] Schmidt P W and Hight R 1960 *Acta Crystallogr.* **13** 480
[16] Weiss R J 1951 *Phys. Rev.* **83** 379